Atmospheric River orientation determines flood occurrence

Received: 1 July 2020 | Accepted: 2 September 2020

DOI: 10.1002/hyp.13905

SCIENTIFIC BRIEFING

HP TODAY WILEY

Atmospheric river orientation determines flood occurrence

Helen V. Griffith[1] | Andrew J. Wade[1] | David A. Lavers[2] | Glenn Watts[3]

[1]Department of Geography and Environmental Science, University of Reading, Reading, UK

[2]Forecast Department, European Centre for Medium-Range Weather Forecasts, Reading, UK

[3]Research Department, Environment Agency, Bristol, UK

Correspondence
Helen V. Griffith, Department of Geography and Environmental Science, University of Reading, Reading, UK.
Email: h.v.griffith@pgr.reading.ac.uk

Funding information
NERC CASE (Environment Agency) Studentship, Grant/Award Number: NE/P010040/1

Abstract

Atmospheric Rivers (ARs) have been linked to many of the largest recorded UK winter floods. These large-scale features can be 500–800 km in width but produce markedly different flood responses in adjacent catchments. Here we combine meteorological and hydrological data to examine why two impermeable catchments on the west coast of Britain respond differently to landfalling ARs. This is important to help better understand flood generation associated with ARs and improve flood forecasting and climate-change impact assessment. Analysis of 32 years of a newly available ERA5 high-resolution atmospheric reanalysis and corresponding 15-min river flow data show that the most impactful ARs arise through a combination of the orientation and magnitude of their water vapour flux. At the Dyfi catchment, AR orientations of between 238–258° result in the strongest hydrological responses, whereas at the Teifi the range is 224–243°. We believe this differential flood response is the result of catchment orientation and topography enhancing or suppressing orographic rainfall totals, even in relatively low-relief coastal catchments. Further to the AR orientation, ARs must have an average water vapour flux of 400–450 kg m^{-1} s^{-1} across their lifetime. Understanding the preferential properties of impactful ARs at catchments allows for the linking of large-scale synoptic features, such as ARs, directly to winter flood impacts. These results using two test catchments suggest a novel approach to flood forecasts through the inclusion of AR activity.

KEYWORDS

atmospheric rivers, catchments, ERA5, flood forecasting, flooding, orographic effect, precipitation, UK

1 | INTRODUCTION

Atmospheric Rivers (ARs) are narrow regions of enhanced low-level moisture transport in mid-latitude cyclones (Browning & Pardoe, 1973; Newell, Newell, Zhu, & Scott, 1992) that are responsible for most of the meridional water vapour transport across the mid-latitudes (Zhu & Newell, 1998). These plumes of warm, moist air can generate very high rainfall totals as they cross elevated terrain and have been linked to floods in many coastal regions of the world (Barth, Villarini, Nayak, & White, 2017; Dettinger, 2011; Kingston, Lavers, & Hannah, 2016; Lavers et al., 2011; Lavers & Villarini, 2013; Paltan et al., 2017; Stohl, Forster, & Sodemann, 2008). The resulting hydrological impact of an AR is both dependent on the characteristics of the AR, such as its duration and intensity, and on the land surface physiography, for example, the bedrock type and terrain (Cao, Mehran, Ralph, & Lettenmaier, 2019; Hecht & Cordeira, 2017;

Neiman, Schick, Ralph, Hughes, & Wick, 2011; Ralph et al., 2019; Ralph, Neiman, Kingsmill, Persson, & White, 2003).

In the UK, ARs are an important cause of floods, with some catchments having up to 80% of their largest winter floods associated with AR events (Lavers et al., 2011; Lavers, Villarini, Allan, Wood, & Wade, 2012). In western Wales, however, two nearby catchments appear to respond very differently to landfalling ARs. These catchments, the Dyfi and the Teifi, are less than 70 km apart, but over the period 1979–2010 in a study of nine catchments along the west coast of Britain (Lavers et al., 2012), they demonstrated the strongest and weakest correlations between landfalling ARs and flood occurrence, respectively. Given the synoptic scale of ARs and their estimated widths of around 500–800 km, which means an AR would most likely affect both catchments, the aim of this study is to understand why these two catchments demonstrate such different hydrological responses to what may be expected a priori to be similar meteorological conditions.

We will use newly available high-resolution atmospheric reanalysis (ERA5; Hersbach et al., 2020) and 15-min flow measurements to probe in finer detail than ever before the relationship between landfalling AR events and extreme flood events. In particular, we are interested in identifying the properties of AR events that may act as pointers towards impact potential. We expect that at this high atmospheric resolution it will be possible to detect the evolution of the AR across the lifetime of the event, pinpointing to a greater accuracy the strength, orientation and location of the landfalling AR water vapour flux. In addition, a significant increase in hydrological resolution will allow a more precise estimate of the timing and magnitude of flood response.

2 | STUDY AREAS AND DATA

2.1 | Dyfi and Teifi catchments

The Dyfi and Teifi catchments (Figure 1) are predominantly rural catchments in western Wales. The River Dyfi (catchment area 471 km^2, average annual rainfall 1834 mm) flows for nearly 50 km through moorland and forestry to its mouth at the Dyfi estuary. The River Teifi (catchment area 890 km^2, average annual rainfall 1,382 mm) flows just over 110 km from a small lake in the upland regions, through moorland to the basin of Cors Caron. From there, it flows through lowland agricultural land until its mouth at Cardigan Bay.

Both catchments have impermeable Silurian period formations predominantly, though the Teifi also includes deposits from the Ordovician. This geology, in combination with the significant altitude ranges found at both catchments, means that the basins are expected to respond quickly to any input rainfall. Differences to note are that the Teifi covers an area nearly twice that of the Dyfi and possesses a

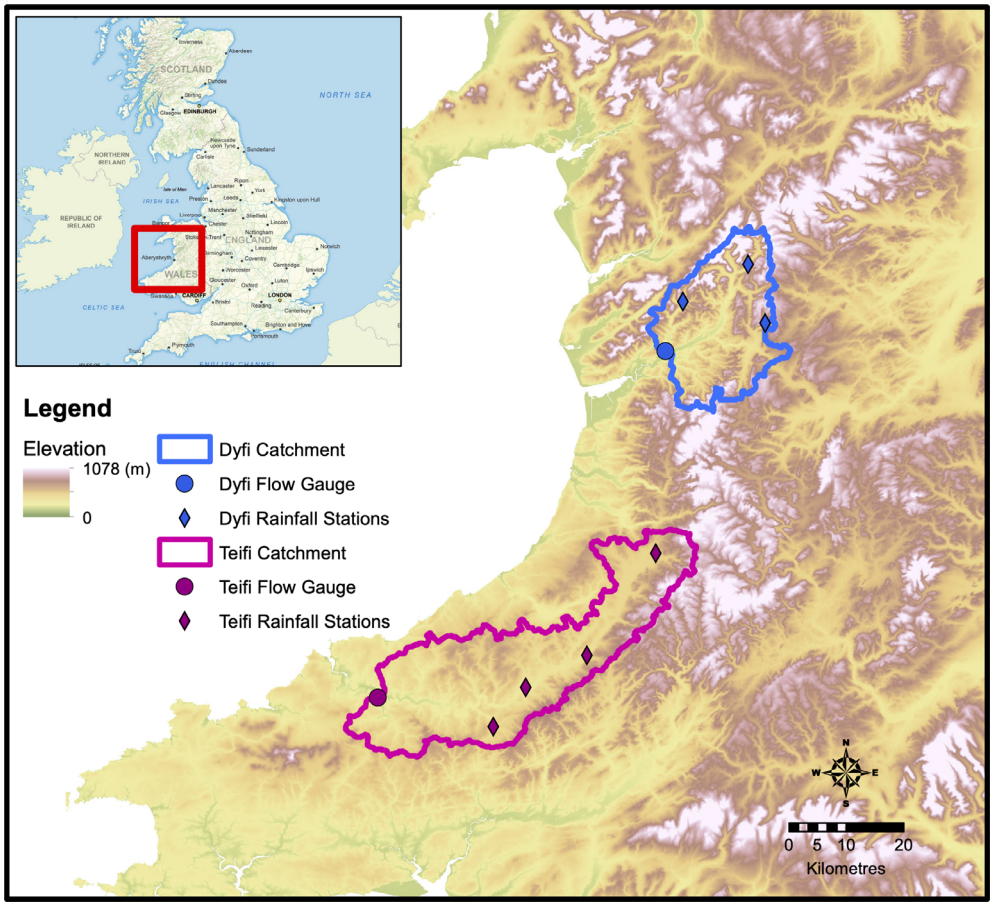

FIGURE 1 The location of the Dyfi and Teifi catchments in Wales. The locations of the flow gauges and precipitation stations are highlighted by the circle and diamond markers respectively. Elevations are from the Institute of Hydrology Digital Terrain Model (IHDTM, Morris & Flavin, 1990, 1994)

more elongated basin shape. The average slopes at the Teifi catchments of 10% are also somewhat shallower than the Dyfi, which has a mean slope gradient of approximately 30%. Due to the location of the catchments in the uplands of the western UK, the catchments are expected to have consistently high soil moisture across the winter period (Lavers, Prudhomme, & Hannah, 2010).

2.2 | Flood selection at the Dyfi and Teifi catchments

Flows were calculated from 15-min stage data at the Dyfi Bridge and Glan Teifi gauging stations (National River Flow Archive) from 1982–2014. The gauging station at Dyfi Bridge underwent major structural change in 2014 and a new rating curve is currently being developed for data after this period. Flood events were extracted via a Peaks-Over-Threshold (POT) analysis for the winter half-year (October–March) for POT3 flood events (on average three floods each year). Summer floods were excluded because they are not normally driven by ARs (Champion, Allan, & Lavers, 2015) and they are generally smaller in magnitude. Following Lavers et al. (2012), a seven-day separation was applied to ensure independence of the flood events.

In addition to the flow data, precipitation data at a 15-min resolution were obtained for three gauging stations in the Dyfi and four stations in the Teifi (Figure 1) to help explore the effect of AR orientation and intensity on the catchment rainfall. Two stations in the near vicinity of the Dyfi and a single station nearby the Teifi were also considered. Rainfall estimates were combined according to Theisen polygons to obtain a measure of basin-averaged AR event total rainfall.

2.3 | AR detection method

Persistent AR events across the winters of 1982–2014 were extracted from the ERA5 reanalysis (Hersbach et al., 2020) at hourly timesteps. ERA5 has a spatial resolution of approximately 0.28 x 0.28°, around a third finer than datasets used in previous analyses (Lavers et al., 2012). The eastward and northward components of the water vapour flux were retrieved across the UK and combined to calculate the vertically-integrated horizontal water vapour transport (hereon Integrated Vapour Transport; IVT), and its associated orientation. Following the steps described by Lavers et al. (2012), at each timestep, we extracted the maximum value of IVT along the British coastline (taken as approximately 4°W) and tested whether a threshold of 500 kg m^{-1} s^{-1} was exceeded. If so, a similar procedure was carried out at the adjacent grid cells in an attempt to trace the IVT plume back across the Atlantic. An AR was identified if the plume could be traced continuously over a distance of more than 20° longitude and for at least 18 hours. Across the 1982–2014 time period, a total of 107 persistent winter ARs were detected (an average of 3–4 ARs per winter). We suggest that the discrepancy between the frequencies of AR events found herein and in Lavers et al. (2012), where an average frequency of 8–10 events per winter was detected, has arisen as a result of the increased ability to detect atmospheric variability in the hourly ERA5 data. For example, temporary drops in IVT along the axis of the AR (Ralph, Neiman, Kiladis, Weickmann, & Reynolds, 2011) across the lifetime of the ARs, possibly due to secondary frontal waves, may have led to a reduced number of ARs being identified. For each AR event, the average IVT magnitude and orientation values were extracted from the ERA5 grid squares containing the location of gauging stations at the Dyfi and Teifi catchments.

3 | RESULTS AND DISCUSSION

3.1 | Atmospheric rivers and POT3 flood events

A POT flood was said to be associated with an AR event if the flood occurred within the 3 days immediately following AR arrival. For the POT3 floods at the Dyfi, 34 out of a possible 96 floods could be linked to ARs. For the Teifi, only 13 of 96 floods could be attributed to ARs. Of the POT3 floods that occurred at both the Dyfi and the Teifi, only 11 were found to be associated with the same AR. It is evident therefore, that the majority of AR events do not affect the catchments in the same way.

3.1.1 | The Dyfi catchment

The distributions of POT3 and non-POT3 AR samples in terms of their landfalling properties are shown in Figure 2 for the Dyfi catchment. Two statistical tests were employed to assess the mean and spread of the two samples; these are the *T*-Test and Levene Test, respectively. The *T*-Test is used to test the null hypothesis that the two samples have equal means and the Levene test is used to test the null hypothesis that the two samples have equal variances. A significant *p*-value (of less than .05) allows us to reject the null hypothesis. In addition, a two-sample Kolmogorov–Smirnov (KS) Test was used to test the null hypothesis that the two samples are drawn from the same (continuous) distribution. The KS test is non-parametric and therefore makes no assumptions regarding the distributions of our samples, however an apparent weakness lies within its ability to detect differences when the samples differ in the extreme values (distribution tails).

In terms of IVT orientation (panel a), the boxplots suggest that the non-POT3 ARs demonstrate a wide range of possible orientations, from 205–310° when considering the entire sample. Conversely, the POT3 flood AR sample demonstrates a much smaller range of 220–280°. Furthermore, by only considering the central 50% of the relevant distributions (i.e., between the upper and lower quartiles), we have identified the POT3 flood generating ARs to demonstate orientations of between 238–258° as compared to 230–268° for the non-POT3 flood generating AR sample. Using the Levene test, we find that there are significant differences between the spread of the two distributions, providing statistical evidence for a preferential orientation of

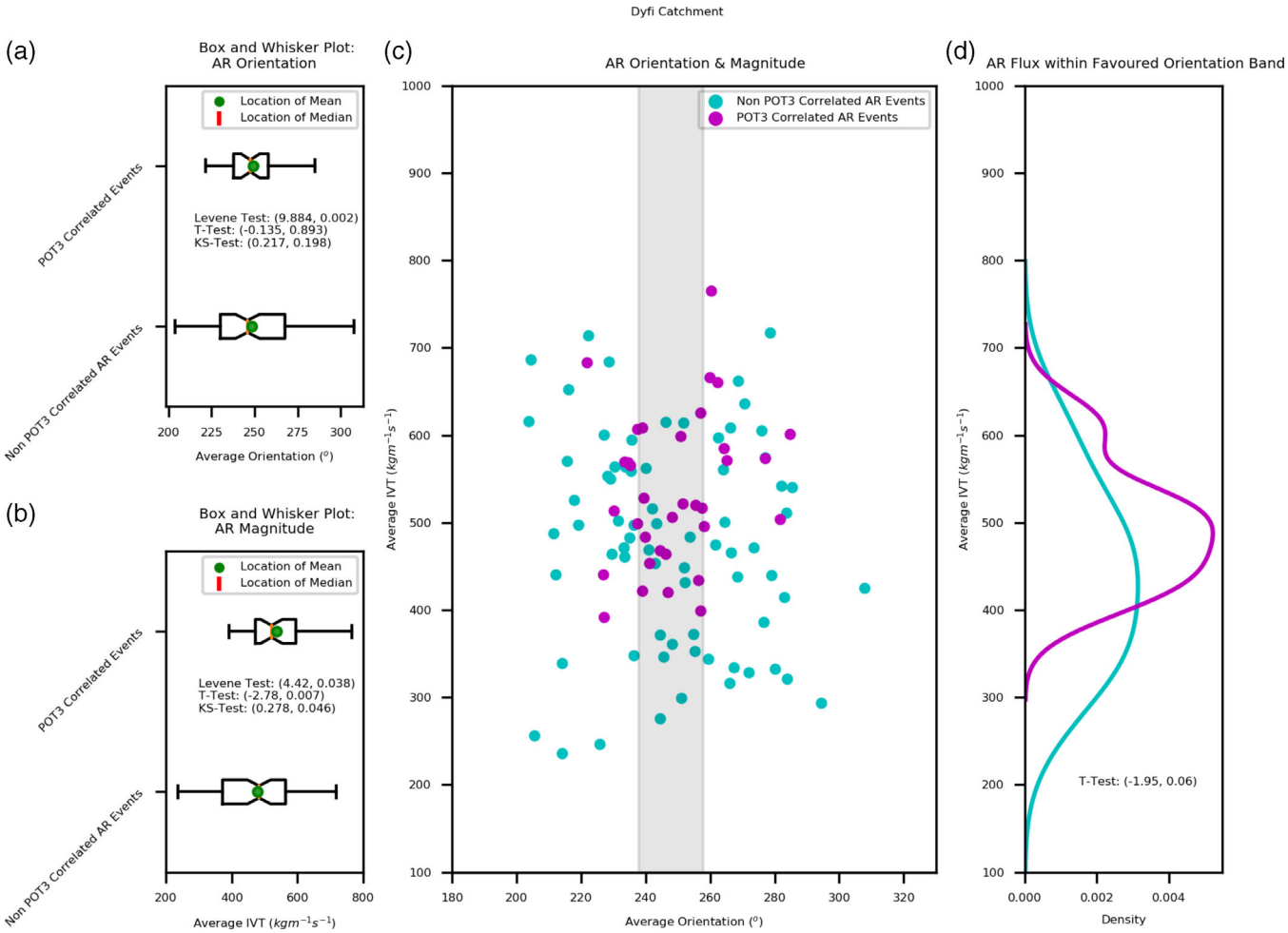

FIGURE 2 The distribution of IVT orientation (panel a) and magnitude (panels b) of POT3 correlated and non- POT3 correlated ARs at the Dyfi catchment. The relevant distributions are described in terms of box and whisker plots; the whiskers correspond to the 5th and 95th percentiles, the boxes bound the 25th and 75th percentiles, and the dot and line within the boxes represent the mean and median respectively. Statistical results in the format (test statistic, p-value) are given in the legend of each subplot. Panels (a) and (b) show the POT3 related ARs to exist preferentially in a subset of possible orientation and magnitude ranges. The Levene and *T*-Tests support the interpretation of preferential orientation and magnitude ranges for ARs that are correlated to POT3 floods. We suggest a possible weakness in the KS test in terms of detecting changes in the extremes of our samples, possibly explaining the lack of significant result in terms of AR orientation. The preferential orientation band is extracted from the bounds of the box plots as 238–258°. Combining the orientation and magnitude dependencies in a simple scatter plot (panel c) and extracting the properties of the AR events to fall within the preferential orientation window (panel d), we identify a threshold in magnitude of 400–450 kg m^{-1} s^{-1} for the POT3 flood generating events

impactful ARs. In terms of IVT magnitude (panel b), the mean IVT for the POT3 events is 536 kg m^{-1} s^{-1} compared to 479 kg m^{-1} s^{-1} for the non-AR group. Using the *T*-Test, we can show that these means are significantly different at the 99% significance level (*p*-value of .007). Hence, the ARs associated with POT3 floods tend to possess greater IVT magnitudes. The KS test does not return a significant result (*p* value >.05) when looking at the distribution of AR orientations and we suggest this is due to the samples differing primarily in the extremes, that is at the Dyfi there is a narrow range of orientations that generate the most significant floods. In agreement with the *T* and Levene Tests, we find that the POT3 flood generating ARs are significantly different in terms of IVT magnitude than those not linked to POT3 floods (*p*-value .046).

We have briefly investigated the sensitivity of the results to different flood thresholds, in particular the POT1 sample. At the Dyfi, a narrower preferential range is found (248–258°) with a significant Levene Test result. However, the smaller sample sizes adversely effect the robustness of our statistical tests in general, and so we choose to focus on the POT3 sample in this study.

The combined relationship between the AR orientation and magnitude for the POT3 correlated sample and non-related POT3 events are shown in panel c of Figure 2. Within the preferential orientation ranges identified above, we identify the mean IVT for the POT3 events to be 500 kg m^{-1} s^{-1} compared to 440 kg m^{-1} s^{-1} for the non-AR group (panel d), with all POT3 flood generating ARs existing above a threshold of 400 kg m^{-1} s^{-1}. Using the T-Test, we can show

that the means of the relevant distributions are different at the 90% significance level (p value of .06), however we note the likelihood of these results changing significantly through a widening of the preferential orientation range to include more AR events.

3.1.2 | The Teifi catchment

As for the Dyfi, at the Teifi catchment (Figure 3), In terms of orientation (panel a), the boxplots referring to the non-POT3 ARs demonstrate a wide range of possible orientations, from 205–310° when considering the entire sample. The similarity to the results for the non-POT3 related ARs of the Dyfi is in line with our expectation of the same AR events impacting the catchments across our study period (given the typical width of landfalling AR events to be on the order of 500–800 km).

Conversely, the POT3 flood AR sample demonstrates a much smaller range of 205–260°. As for the Dyfi catchment, the existence of a narrower distribution of the AR POT3 floods suggests a preferential orientation. Furthermore, by only considering the central 50% of the distribution (i.e., between the upper and lower quartiles), we have identified the central 50% of the POT3 flood generating ARs to exist between 224–243° as compared to 233–266° for the non-POT3 sample. The Levene Test again provides statistical evidence that the spread of the POT3 and non-POT3 AR distributions are different at the 95% significance level (p-value .002). Similar to our findings at the Dyfi catchment, the average IVT of the POT3 ARs is greater than that of the non-POT3 sample, 567 kg m^{-1} s^{-1} compared to 515 kg m^{-1} s^{-1}

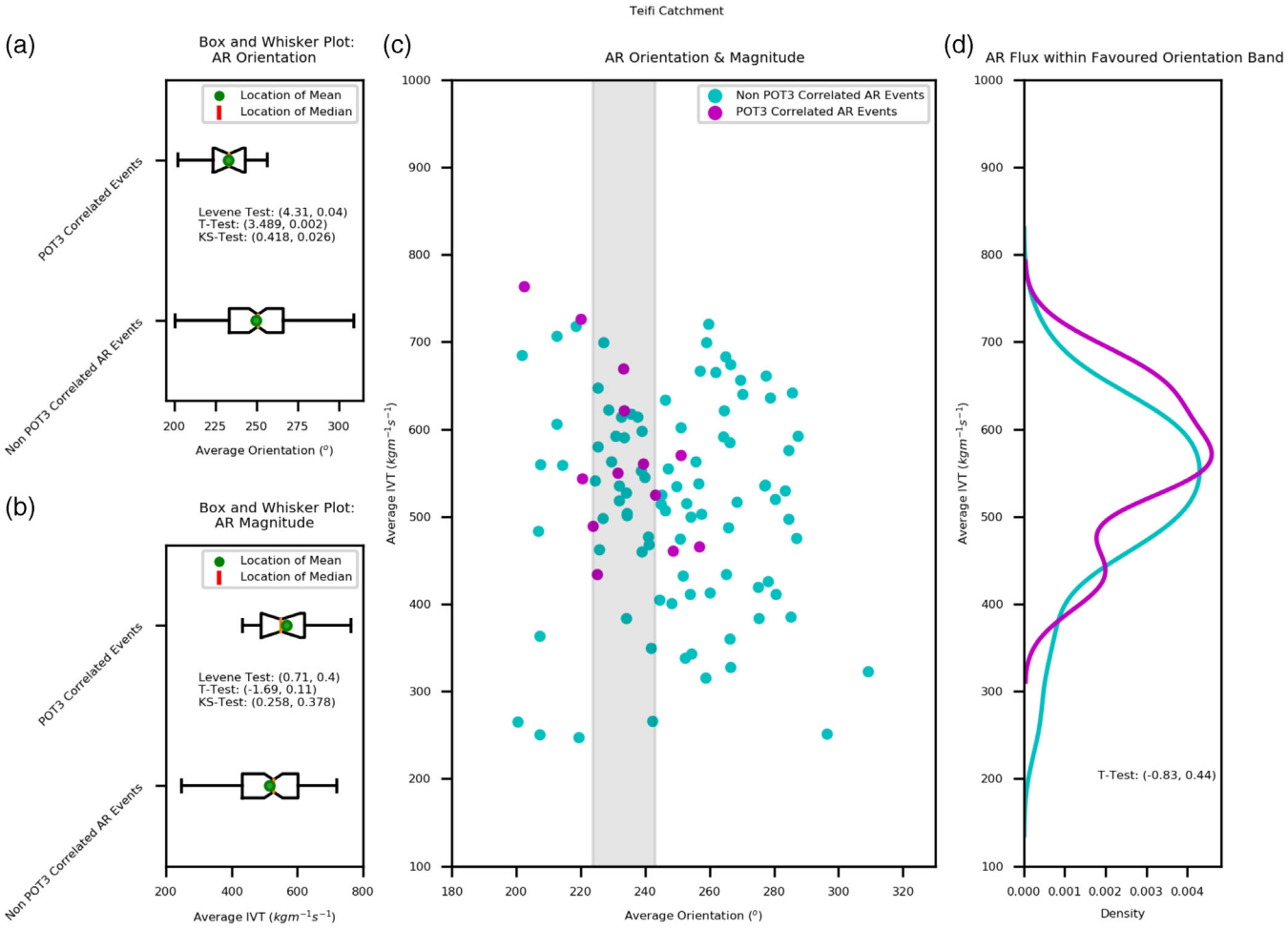

FIGURE 3 The distribution of IVT orientation (panel a) and magnitude (panels b) of POT3 correlated and non-POT3 correlated ARs at the Teifi catchment. As in Figure 2, the relevant distributions are described in terms of box and whisker plots; the whiskers correspond to the 5th and 95th percentiles, the boxes bound the 25th and 75th percentiles, and the dot and line within the boxes represent the mean and median respectively. Statistical results in the format (test statistic, p-value) are given in the legend of each subplot. Panel (a) shows the POT3 related ARs to exist preferentially in a subset of possible orientation ranges. The results of the Levene, KS and T-tests support this interpretation. We find a preferential orientation band of 224–243° for the POT3 flood generating ARs. Although the POT3 flood generating ARs show a similar skew towards stronger IVT magnitudes, this result is less clear in the statistical tests than for the Dyfi catchment (Figure 2). We note this could be due to the smaller sample sizes at the Teifi catchment as compared to the Dyfi. Combining the orientation and magnitude dependencies (panel c) and extracting the properties of the AR events to fall within the preferential orientation window (panel d), we are able to identify a similar threshold in magnitude of 400–450 kg m^{-1} s^{-1} for the POT3 flood generating AR events

(panel b). We suggest the smaller sample sizes may at least partly explain the absence of a significant difference in these means; the Teifi catchment demonstrates fewer POT3 correlated ARs as compared to the Dyfi. In agreement with earlier results, the KS test suggests that the POT3 flood generating ARs are significantly different in terms of IVT orientation than those not linked to POT3 floods (*p*-value .026).

At the Teifi catchment when considering a similar analysis for the POT1 floods, an orientation range similar to that above is found, however the statistical analyses are much less robust. This is likely a result

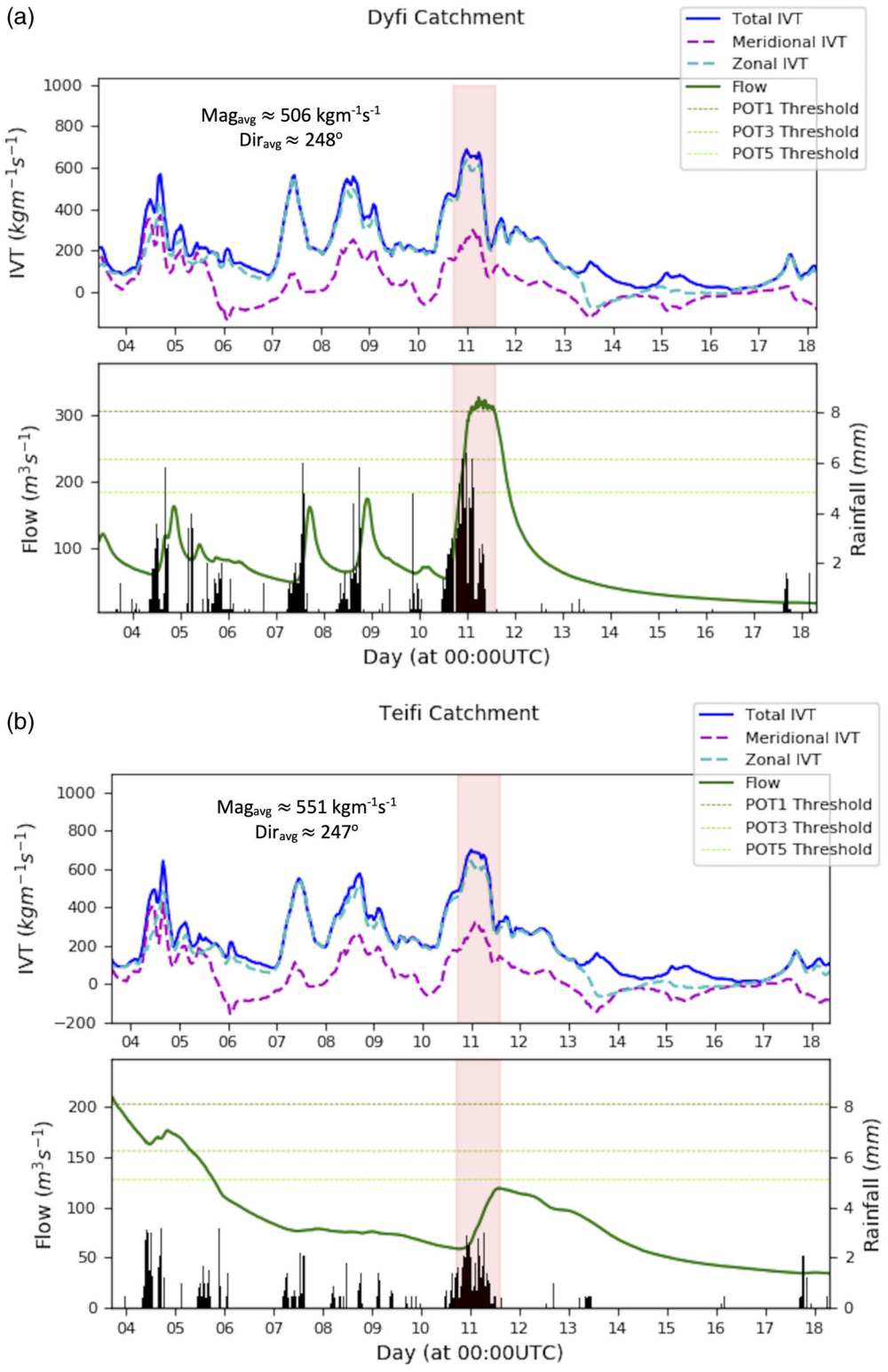

FIGURE 4 Time series analysis of landfalling IVT, rainfall and flow patterns at the Dyfi and Teifi catchments in response to an AR on the 11th February 2002 (red shaded region). The average magnitude and orientation properties of the AR are shown. We suggest the difference in flood responses between the catchments can be explained through the AR magnitude and orientation. The AR orientation of 247° sits outside the preferential range identified at the Teifi catchment of 224–243° but inside that of the Dyfi (238–258°). We see a stronger impact on flow at the Dyfi compared to the Teifi, despite the average IVT magnitude at the Dyfi being smaller than that at the Teifi. This suggests AR orientation is an important control on rainfall occurrence, and therefore flood response

of the sample sizes (only seven ARs can be correlated to POT1 floods at the Teifi).

The combined relationship between the AR orientation and magnitude for the POT3 correlated sample and non-related POT3 events are shown in panel c of Figure 3. Within the preferential orientation ranges identified above, we identify the mean IVT for the POT3 events to be 567 kg m^{-1} s^{-1} compared to 530 kg m^{-1} s^{-1} for the non-AR group (panel d), with all POT3 flood generating ARs existing above the 450 kg m^{-1} s^{-1} threshold. As compared to the Dyfi catchment, there appears to be less of a skew towards stronger magnitude IVT ARs when considering the most impactful events. We suggest this is primarily a result of small sample sizes at the Teifi catchment as a visual trend is apparent.

3.2 | Case study application: AR of 10th - 11th February 2002

The findings of Section 3.1 are exemplified in a case study. Figure 4 shows the evolution of overhead IVT flux components (both the total magnitude and zonal (eastward) and meridional (northward)) and flow/precipitation observations at the Dyfi and Teifi catchments across the month of February 2002. The incident AR (highlighted by the shaded section in Figure 4) was found to demonstrate an average magnitude of 506 kg m^{-1} s^{-1} at the Dyfi catchment and 551 kg m^{-1} s^{-1} at the Teifi. The orientation of the landfalling flux was calculated as 248° at the Dyfi and 247° at the Teifi. In line with the findings of Section 3.1 and the presence of AR orientation as a primary control on AR impact potential, the AR results in a much more significant response at the Dyfi catchment as compared to the Teifi.

4 | CONCLUSIONS AND FUTURE WORK

This study has used high-resolution datasets to link the large-scale atmospheric conditions directly to local flood peaks. The main control on impactful ARs at these two flashy catchments in western Wales has been found to be the orientation of the incoming IVT relative to catchment topography. At the Dyfi catchment, the POT3 flood generating ARs demonstrate average IVT flux orientations of 238–258° across their lifetimes, whereas at the Teifi a range of 224–243° is preferred. These results are summarized in the Figure 5 schematic.

We suggest that at the Dyfi, surrounded by the mountains of Snowdonia, ARs that follow the main river channel have the most impact potential in terms of flood generation and magnitude. This seems to be the result of "rainout" as the AR hits the higher elevation land at the head of the valley (Ralph et al., 2003). When these ARs have an IVT above 400–450 kg m^{-1} s^{-1}, the largest floods (POT3 and above) can occur. In the Teifi, which is a less mountainous catchment, this effect is also apparent. We suggest this to be the topographic effect of the northern edge of the catchment lowlands and/or IVT into the upland regions.

A next step is to confirm the processes and establish the strength of this effect at a national level. We are aware of several limitations

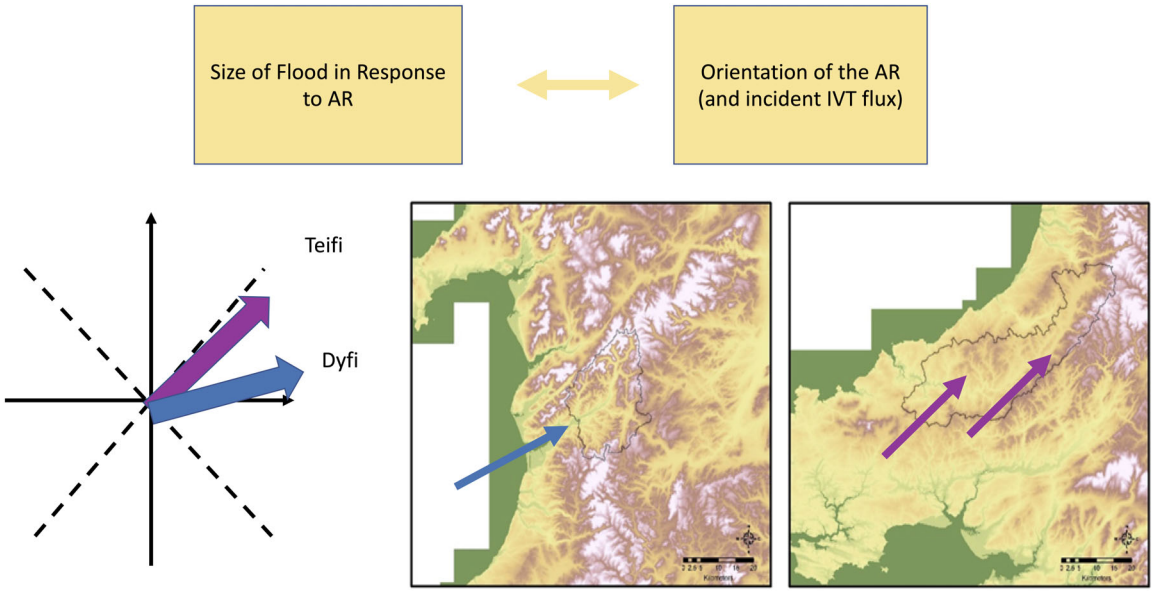

FIGURE 5 Summary schematic of our conclusions. We suggest the primary control on AR impact lies with the orientation of the landfalling flux relative to catchment slopes. We suggest physically this can be interpreted as the efficiency of orographic enhancement of the landfalling AR and the amount of precipitation induced. When the orientation of the AR is preferable, the extent of response lies with the amount of moisture transported towards the catchment that is, the IVT magnitude. We suggest that the ARs associated with the largest floods possess average IVT magnitudes above 400–450kg m^{-1} s^{-1}. Elevations are from the Institute of Hydrology Digital Terrain Model (IHDTM, Morris & Flavin, 1990, 1994)

and restrictions inherent to the current AR detection algorithm that are likely to be filtering out legitimate ARs, as several POT3 floods at these catchments showed traces of precursor AR events. For example, we hypothesize that we are not currently detecting ARs with secondary frontal wave activity. It is likely therefore that we are missing some AR events when dealing with high-resolution input data such as ERA5. This does not alter the result reported here, but points the way in terms of the next step for further refinement; if work can be done to increase the resilience and effectiveness of the detection algorithm, and if preferential AR orientations can be calculated for a greater variety of catchments, then this offers great potential for the improved forecasting of extreme flood events (Lavers, Pappenberger, & Zsoter, 2014; Ramos, Sousa, Dutra, & Trigo, 2020). In the future, forecasts based on likely AR properties could improve the identification of damaging storms, potentially reducing impact to people and property.

ACKNOWLEDGEMENTS

We thank Natural Resources Wales for kindly providing the river flow and precipitation data. The work was funded jointly by the UK Natural Environment Research Council and the Environment Agency under award code NE/P010040/1. The views expressed are those of the authors and not the organisations for which they work. We acknowledge the anonymous reviewers who provided useful comments on the manuscript.

DATA AVAILABILITY STATEMENT

Hydrological and Precipitation Datasets from Natural Resources Wales (NRW) ERA5 from Copernicus Climate Change Service (C3S).

ORCID

Helen V. Griffith https://orcid.org/0000-0001-8338-0149

REFERENCES

Barth, N. A., Villarini, G., Nayak, M. A., & White, K. (2017). Mixed populations and annual flood frequency estimates in the western United States: The role of atmospheric rivers. *Water Resources Research*, *53*(1), 257–269. https://doi.org/10.1002/2016WR019064

Browning, K. A., & Pardoe, C. W. (1973). Structure of low-level jet streams ahead of mid-latitude cold fronts. *Quarterly Journal of the Royal Meteorological Society*, *99*(422), 619–638. https://doi.org/10.1002/qj.49709942204

Cao, Q., Mehran, A., Ralph, F. M., & Lettenmaier, D. P. (2019). The role of hydrological initial conditions on Atmospheric River floods in the Russian River basin. *Journal of Hydrometeorology*, *20*(8), 1667–1686. https://doi.org/10.1175/JHM-D-19-0030.1

Champion, A., Allan, R. P., & Lavers, D. A. (2015). Atmospheric rivers do not explain UKsummer extreme rainfall. *Journal of Geophysical Research: Atmospheres*, *120*(14), 6731–6741.

Dettinger, M. (2011). Climate change, atmospheric Rivers, and floods in California - a multimodel analysis of storm frequency and magnitude Changes1: Climate change, atmospheric Rivers, and floods in California—A multimodel analysis of storm frequency and magnitude changes. *JAWRA Journal of the American Water Resources Association*, *47*(3), 514–523. https://doi.org/10.1111/j.1752-1688.2011.00546.x

Hecht, C. W., & Cordeira, J. M. (2017). Characterizing the influence of atmospheric river orientation and intensity on precipitation distributions over north coastal California: ARs and precipitation over north coastal CA. *Geophysical Research Letters*, *44*(17), 9048–9058. https://doi.org/10.1002/2017GL074179

Hersbach, H., Bell, B., Berrisford, P., Hirahara, S., Horányi, A., Muñoz-Sabater, J., … Thépaut, J. (2020). The ERA5 global reanalysis. *Quarterly Journal of the Royal Meteorological Society*, *146*, 1999–2049. https://doi.org/10.1002/qj.3803

Kingston, D. G., Lavers, D. A., & Hannah, D. M. (2016). Floods in the southern Alps of New Zealand: The importance of atmospheric Rivers: Atmospheric Rivers and floods in New Zealand. *Hydrological Processes*, *30*(26), 5063–5070. https://doi.org/10.1002/hyp.10982

Lavers, D., Prudhomme, C., & Hannah, D. M. (2010). Large-scale climate, precipitation and British river flows: Identifying hydroclimatological connections and dynamics. *Journal of Hydrology*, *395*(3-4), 242–255. https://doi.org/10.1016/j.jhydrol.2010.10.036

Lavers, D. A., Allan, R. P., Wood, E. F., Villarini, G., Brayshaw, D. J., & Wade, A. J. (2011). WINTER floods in Britain are connected to atmospheric rivers: UK winter floods and atmospheric rivers. *Geophysical Research Letters*, *38*, L23803. https://doi.org/10.1029/2011GL049783

Lavers, D. A., Pappenberger, F., & Zsoter, E. (2014). Extending medium-range predictability of extreme hydrological events in Europe. *Nature Communications*, *5*(1), 5382. https://doi.org/10.1038/ncomms6382

Lavers, D. A., & Villarini, G. (2013). The nexus between atmospheric rivers and extreme precipitation across Europe: ARs and extreme European precipitation. *Geophysical Research Letters*, *40*(12), 3259–3264. https://doi.org/10.1002/grl.50636

Lavers, D. A., Villarini, G., Allan, R. P., Wood, E. F., & Wade, A. J. (2012). The detection of atmospheric rivers in atmospheric reanalyses and their links to British winter floods and the large-scale climatic circulation. *Journal of Geophysical Research: Atmospheres*, *117*, D20106. https://doi.org/10.1029/2012JD018027

Morris, D. G., & Flavin, R. W. (1990). A digital terrain model for hydrology. *Proc 4th International Symposium on Spatial Data Handling*, *1*, 250–262.

Morris, D. G., & Flavin, R. W. (1994). *Sub-set of the UK 50 m by 50 m hydrological digital terrain model grids*. Wallingford, England: NERC, Institute of Hydrology.

Neiman, P. J., Schick, L. J., Ralph, F. M., Hughes, M., & Wick, G. A. (2011). Flooding in Western Washington: The connection to atmospheric Rivers. *Journal of Hydrometeorology*, *12*(6), 1337–1358. https://doi.org/10.1175/2011JHM1358.1

Newell, R. E., Newell, N. E., Zhu, Y., & Scott, C. (1992). Tropospheric rivers? A pilot study. *Geophysical Research Letters*, *19*(24), 2401–2404. https://doi.org/10.1029/92GL02916

Paltan, H., Waliser, D., Lim, W. H., Guan, B., Yamazaki, D., Pant, R., & Dadson, S. (2017). Global floods and water availability driven by atmospheric Rivers: Global hydrology and ARs. *Geophysical Research Letters*, *44*(20), 10387–10395. https://doi.org/10.1002/2017GL074882

Ralph, F. M., Neiman, P. J., Kiladis, G. N., Weickmann, K., & Reynolds, D. W. (2011). A multiscale observational case study of a Pacific Atmospheric River exhibiting tropical–extratropical connections and a mesoscale frontal wave. *Monthly Weather Review*, *139*(4), 1169–1189. https://doi.org/10.1175/2010MWR3596.1

Ralph, F. M., Neiman, P. J., Kingsmill, D. E., Persson, P. O. G., & White, A. B. (2003). The impact of a prominent rain shadow on flooding in California's Santa Cruz Mountains: A CALJET case study and sensitivity to the ENSO cycle. *Journal of Hydrometeorology*, *4*, 22.

Ralph, F. M., Rutz, J. J., Cordeira, J. M., Dettinger, M., Anderson, M., Reynolds, D., … Smallcomb, C. (2019). A scale to characterize the strength and impacts of atmospheric Rivers. *Bulletin of the American Meteorological Society*, *100*(2), 269–289. https://doi.org/10.1175/BAMS-D-18-0023.1

Ramos, A. M., Sousa, P. M., Dutra, E., & Trigo, R. M. (2020). Predictive skill for atmospheric rivers in the western Iberian Peninsula. *Natural Hazards and Earth System Sciences*, *20*(3), 877–888. https://doi.org/10.5194/nhess-20-877-2020

Stohl, A., Forster, C., & Sodemann, H. (2008). Remote sources of water vapor forming precipitation on the Norwegian west coast at 60°N–a tale of hurricanes and an atmospheric river. *Journal of Geophysical Research: Atmospheres*, *113*, D05102. https://doi.org/10.1029/2007JD009006

Zhu, Y., & Newell, R. E. (1998). A proposed algorithm for moisture fluxes from atmospheric Rivers. *Monthly Weather Review*, *126*, 11.

How to cite this article: Griffith HV, Wade AJ, Lavers DA, Watts G. Atmospheric river orientation determines flood occurrence. *Hydrological Processes*. 2020;1–9. https://doi.org/10.1002/hyp.13905